Evaluation of Transport-Equations-Based Transition Models for High-Speed Boundary Layers Using OVERFLOW

Ethan A. Vogel* and Meelan Choudhari†
NASA Langley Research Center, Hampton, VA, 23681

Balaji Shankar Venkatachari‡
National Institute of Aerospace, Hampton, VA 23666

Accurate modeling of laminar-turbulent transition is crucial for the design of hypersonic flight systems. However, the current transition models used in production CFD codes are insufficient for high-speed flows. Many extensions to low-speed models have been suggested; however, a thorough verification and validation effort is needed before these models can be used in design settings. Challenges include potentially missing details of the model implementation requirements and/or a complete specification of the input parameters needed to replicate the test findings. A meaningful assessment of the generalization capability of these models is also hindered by a lack of information regarding the specific flow configurations and associated grids employed for model calibration. As a key first step toward model verification, we present an independent assessment of two recently proposed models for high-speed transition, namely, a model within the SST-γ framework and a model based on the SST-$\gamma - \nu_L$ equations. These models are implemented in the NASA OVERFLOW 2.3e solver and their performance in predicting first mode, second mode, and crossflow transition has been evaluated for several test cases in the supersonic and hypersonic regimes. Besides the test cases employed by the model developers, which could have also been used for model calibration, the present assessment includes supplementary configurations that contribute to an unbiased assessment of the models. The outcomes presented in this study indicate the potential for the models to be applied to high-speed flight configurations. Key steps toward future improvements to these models are also outlined.

Nomenclature

a	=	Local sonic speed (nondimensionalized by free-stream speed of sound)
C_f	=	Local skin friction coefficient (nondimensional)
$C_1, C_2, C_3, C_{f,crit}$	=	Constants in γ equation (nondimensional, Table 1)
d	=	Distance to location of nearest wall (nondimensionalized by grid unit length)
D_γ	=	Destruction of intermittency
D_k	=	Destruction of turbulent kinetic energy
F_{onset}	=	Transition onset function (nondimensional, Eqn. 17)
H	=	Boundary layer shape factor (nondimensional)
k	=	Turbulent kinetic energy (nondimensionalized by free-stream speed of sound)
L	=	Flow length scale (nondimensional), equal to grid unit length
M	=	Mach number (nondimensional parameter)
M_t	=	Turbulence Mach number (nondimensional)
P	=	Pressure (nondimensionalized by free-stream pressure as in Eqn. 24))
P_γ	=	Production of intermittency
P_k	=	Production of turbulent kinetic energy
R	=	Specific gas constant (nondimensionalized by free-stream gas constant)

*Aerospace Technologist, Computational AeroSciences Branch, ethan.a.vogel@nasa.gov, AIAA Member
†Aerospace Technologist, Computational AeroSciences Branch, m.m.choudhari@nasa.gov, AIAA Fellow
‡Sr. Research Engineer, balaji.s.venkatachari@nasa.gov, Senior AIAA Member

R_T	=	Relaminarization function for hypersonic γ model (Eqn. 18)
Re_θ	=	Reynolds number based on momentum thickness (nondimensional parameter)
Re_∞	=	Freestream reference Reynolds number (nondimensional parameter)
S	=	Strain rate magnitude (nondimensionalized by free-stream speed of sound)
T	=	Temperature (nondimensionalized by free-stream temperature)
Tu	=	Turbulence intensity (%)
t	=	Time scale (nondimensionalized by free-stream flow time scale, which is $\frac{a^*}{L^*}$)
u	=	Flow velocity (nondimensionalized by free-stream speed of sound)
x	=	Spatial position (nondimensionalized by grid unit length)
y^+	=	Nondimensional viscous wall spacing
α	=	SST production constant (nondimensional)
β	=	SST production constant (nondimensional)
γ	=	Intermittency (nondimensional)
θ	=	Boundary layer momentum thickness (nondimensionalized by grid unit length)
$\Pi_{cc,k}$	=	Compressibility correction term for SST ω equation
ρ	=	Fluid density (nondimensionalized by free-stream fluid density)
μ	=	Laminar dynamic viscosity (nondimensionalized by free-stream laminar dynamic viscosity)
μ_t	=	Turbulent eddy dynamic viscosity (nondimensionalized by free-stream laminar dynamic viscosity)
ν	=	Laminar kinematic viscosity (nondimensionalized by free-stream laminar kinematic viscosity)
ν_t	=	Turbulent eddy kinematic viscosity (nondimensionalized by free-stream laminar kinematic viscosity)
τ_L	=	laminar fluctuation time scale (nondimensional)
τ_1	=	1^{st} mode time scale (nondimensional)
τ_2	=	2^{nd} mode time scale (nondimensional)
τ_{cf}	=	crossflow mode time scale (nondimensional)
ω	=	Specific turbulence dissipation rate (nondimensional)
Ω	=	Local vorticity magnitude (nondimensionalized by free-stream speed of sound and length)
subscripts		
∞	=	Freestream value
superscripts		
$+$	=	Defined in wall coordinates
$*$	=	Dimensional quantity defined in appropriate SI units
accents		
$\overline{Q}$	=	Mean valued quantity
$\widetilde{Q}$	=	Modified compressibility correction quantity

I. Background and Motivation

Prediction of laminar-to-turbulent transition is a critical capability for the design of high-speed flow systems because transitional and turbulent flows impart additional heat loads to flight systems compared to laminar flows. Often, for industrial-scale CFD calculations the prediction of laminar-to-turbulent transition is accomplished via transport equation-based transition models. These auxiliary transport equations are solved alongside the flow and turbulence model equations and track quantities related to the laminar-turbulent state of the flow with the goal of predicting transition. Presently, there are multiple transition models commonly used in production CFD. Of these, the most prolific are the Langtry-Menter $\gamma - Re_\theta$ [1], Menter γ [2] transition models coupled to the Menter SST turbulence model [3] and the Coder-Maughmer Amplification Factor Transport (AFT) model [4] coupled to the Spalart-Allmaras turbulence model [5].

Most of these models were first developed with the goal of predicting transition in low-speed flows due to Tollmien-Schlicting (TS) instabilities and, in some cases, were later extended to include transition due to crossflow instabilities. However, the transition correlations underlying these models become invalid for high-speed configurations. At higher speeds, Mack's first and second mode come into play and additional effects such as entropy layers due to nose bluntness, surface temperature effects, and bypass transition due to surface roughness also become important [6]. The transition modules currently included in popular CFD solvers are insufficient to analyze these flows.

In recent years, a significant number of candidate models have been suggested to address this gap. Examples of these new models can be found in Refs, [7–13], which represent a subset of what has been proposed in the literature.

However the pace of new model development has exceeded the ability of CFD code developers to implement, validate, and verify them. This has prevented an independent verification of the results presented in the original presentation of a number of models.

This work seeks to begin addressing this gap. In this work, two chosen high-speed transition models are implemented in the OVERFLOW 2.3e flow solver [14] maintained by the NASA Langley Research Center (LaRC). This work contextualizes and describes the chosen models and the details of their implementation in OVERFLOW. Transition predictions made by this model are presented and discussed, and the work remaining to develop models to meet the needs of the hypersonics design community is examined. The remainder of this work is outlined as follows: First, a description of the SST turbulence model is provided. Next, a brief summary of both transition models examined here is given. Next, the test cases of interest in this work are discussed. Finally, results for these test cases are presented and the conclusions reached based on them are outlined. Finally, a description of recommended future efforts is given.

II. Transition Modeling within the Menter SST Framework

All transition models considered in this work are developed for use within the Menter shear-stress transport SST [3] turbulence modeling framework. The SST model has been used extensively for all speed regimes and is not the focus of this work, but a brief description of the model is presented so that the transition models, which are the primary focus of this work, can be understood. The discussion here is intended to provide a high-level summary of the SST model and the models being examined to provide context for the results obtained here. For a complete description of the transition models being analyzed, the reader is referred to the original description of them [7, 8, 11] as well as [15]. In this section, a brief explanation of OVERFLOW's variable nondimensionalization conventions is provided, followed by an overview of the SST turbulence model to which all transition models discussed here are coupled. Finally, a brief discussion of the SST-γ and SST-γ-ν_L transition models is provided.

A. Variable Nondimensionalizations

In all subsequent sections, the variables presented will be nondimensionalized according to the standard nondimensionalizations used by the OVERFLOW solver. Because of this, some equations included herein will differ slightly from the corresponding equations in Refs. [7] or [11]. For ideal gas simulations, the specific gas constant is normalized by its freestream value, and the length scale of the flow is normalized by one grid unit. The consequence of this convention is that these quantities are globally equal to unity, as in

$$L = \frac{L^*}{L_r^*} = 1.0, \qquad R = \frac{R^*}{R_r^*} = 1.0, \tag{1}$$

where the subscript r denotes reference quantities and the superscript * denote dimensional quantities. The relevant nondimensionalizations are

$$x = \frac{x^*}{L_r^*}, \qquad u = \frac{u^*}{a_r^*}, \qquad t = \frac{t^* a_r^*}{L_r^*}, \qquad \rho = \frac{\rho^*}{\rho_r^*}, \qquad \mu = \frac{\mu^*}{\mu_r^*}, \qquad T = \frac{T*}{T_r^* \gamma_g}, \tag{2}$$

where the reference quantities for the dependent variables are the free-stream dimensional values unless otherwise stated. The nondimensional freestream values, identified with the subscript ∞, are used in the model to calculate the boundary-layer edge conditions in subsequent sections. The other nondimensionalizations can be found in Ref. [14], as only those that are relevant to this discussion are included here. These nondimensionalizations yield modified definitions of some derived quantities, including the turbulence modeling variables. The turbulence modeling variables here are nondimensionalized according to

$$k = \frac{k^*}{a_r^{*2}}, \qquad \omega = \frac{\rho k}{\mu_t} Re_r = \frac{\mu_r^*}{\rho_r^* a_r^{*2}} \frac{\rho^* k^*}{\mu_t^*} Re_r = \frac{\omega^*}{a_r^*} \tag{3}$$

and γ, being a nondimensional variable, requires no nondimensionalization. The factor of Re_r in the definition of ω maintains appropriate scaling for that quantity.

B. SST Turbulence Modeling Equations

Transition models can be coupled to the SST turbulence modeling equations via the intermittency, γ, which (loosley) corresponds to the fraction of time the local flow is turbulent at a given point in space. The role of the transition model

is to calculate γ at each point in the flow. The coupling of the transition model to the turbulence modeling equations is accomplished via the inclusion of γ in the production and dissipation terms of the SST transport equation for the turbulent kinetic energy, k. The transitional SST equations may be described in general as

$$\frac{\partial(\rho k)}{\partial t} + \frac{\partial(\rho u_j k)}{\partial x_j} = \gamma P_k - \gamma_{lim} D_k + \Pi_{cc,k} + \frac{1}{Re_\infty}\frac{\partial}{\partial x_j}\left[(\mu + \sigma_k \mu_t)\frac{\partial k}{\partial x_j}\right] \tag{4}$$

$$\frac{\partial(\rho\omega)}{\partial t} + \frac{\partial(\rho u_j \omega)}{\rho x_j} = \alpha\frac{P_k}{\nu_t} - \widetilde{\beta}\rho\omega^2 + \Pi_{cc,\omega} + 2(1-F_1)\frac{\rho\sigma_{\omega 2}}{\omega}\frac{\partial k}{\partial x_j}\frac{\partial \omega}{\partial x_j} + \frac{1}{Re_\infty}\frac{\partial}{\partial x_j}\left[(\mu + \sigma_\omega \mu_t)\frac{\partial \omega}{\partial x_j}\right] \tag{5}$$

where

$$\gamma_{lim} = max(\gamma, 0.1), \tag{6}$$

and the ω equation is unchanged with respect to the original SST equations. In reviewing the SST equations, attention must be given to the chosen form of the compressibility correction. In the release version of OVERFLOW, the Sarkar correction as described in Ref. [16] is used. For high-speed cases, this correction, discussed in detail in Ref. [16] is important for achieving quality simulation results. In this work, the correction is modified in OVERFLOW to the correction verbatim from Refs. [7] and [11], the dilatation term in Eq. 5 is removed, e.g. $\Pi_{cc,\omega} = 0$. Additionally, Eq. 4 is modified for compressibility by

$$\Pi_{cc,k} = -0.15\gamma P_k M_t + 0.2 * \widetilde{\beta^+}\rho\omega k M_t^2, \tag{7}$$

where

$$\widetilde{\beta^+} = \beta^+ + \beta^+\frac{M_t^2}{2}, \tag{8}$$

and

$$\widetilde{\beta} = \beta - \widetilde{\beta^+}\frac{M_t^2}{2}. \tag{9}$$

The recently developed SST-γ [7] and SST-γ-ν_L [11] transition models for high-speed flows are coupled to the SST turbulence models as described in Eqns. 4 and 5. In these equations, α, σ_k, σ_ω, and $\sigma_{\omega 2}$ are SST coefficients, which are subject to blending via the F_1 function between an "inner" and "outer" constant value. None of these constants is altered in the process of coupling turbulence models with the SST equations. Reference [16] provides further description of the constants used in the SST model, including those appearing in the compressiblity correction to this model.The quantity F_1 in Eqn. 5 represents the SST blending function modified by Langtry and Menter [1]. All models implemented into the release version of OVERFLOW are coupled with SST 2003 [3], but the models discussed here are coupled to the 1994 version of SST [17] for consistency with Refs. [7] and [11]. When the models are added to the release distribution of OVERFLOW, they will likely be coupled to the 2003 version of the model, and the sensitivity of each model to the choice of SST version is examined in this work. The 2003 update to the SST model differs from the original in the values of some blending constants, the definition of turbulent eddy viscosity, and the maximum local value of the production of k.

C. SST-γ Transition Model of Liu et al. [7]

The first transition model implemented during the current effort is the one-equation γ model [7] integrated with Menter's SST turbulence model [3]. This is a γ model, meaning the added governing equation predicts the transport of the intermittency factor γ.The implementation of the γ model for high-speed flows uses OVERFLOW version 2.3e that has been modified to include the Menter γ model for transition in low-speed flows. This OVERFLOW implementation is described in detail in Gosin et al. [18]. The correlations used in the development of the high-speed γ model involve flat plate boundary layer similarity solutions, and the model correlations are based on estimated boundary layer edge quantities. The nondimensional γ transport equation is

$$\frac{\partial(\rho\gamma)}{\partial t} + \frac{\partial(\rho u_j \gamma)}{\rho x_j} = P_\gamma - D_\gamma + \frac{1}{Re_r}\frac{\partial}{\partial x_j}\left[(\mu + \mu_t)\frac{\partial \gamma}{\partial x_j}\right] \tag{10}$$

where $j = 1 - 3$ corresponds to the three spatial directions. The production and destruction/relaminarization terms are

$$P_\gamma = C_1\rho S F_{onset}\gamma(1-\gamma) \tag{11}$$

Table 1 Modeling constants for γ transport equations.

C_1	C_2	C_3	$C_{(cf,crit)}$
100.0	0.06	50.0	24.0 (quiet) or 46.0 (noisy)

and

$$D_\gamma = C_2 \rho \Omega F_{turb} \gamma (C_3 \gamma - 1), \tag{12}$$

respectively. Between iterations, a limiter of $0.02 \leq \gamma \leq 1.0$ is enforced, consistent with the description in Ref. [7]. All modeling constants for the γ transport equation can be found in Table 1.

Similar to the Langtry-Menter SST transition model [1] and Menter et al. SST-γ transition model [2], production and destruction of the turbulence index is controlled by onset and turbulence functions, F_{onset} and F_{turb}. In this model, the nondimensional equations take the form

$$F_{onset} = max(F_{onset2} - F_{onset3}, 0) \tag{13}$$

and

$$F_{turb} = exp\left[-(R_T/2)^2\right]. \tag{14}$$

The constituent functions necessary to calculate Eqns 13 and 14 are

$$F_{onset3} = max(1 - (R_T/3.5)^3, 0), \tag{15}$$

$$F_{onset2} = min(max(F_{onset1}, F_{onset1}^4), 2.0), \tag{16}$$

$$F_{onset1} = max(F_{onset,s}, F_{onset,cf}), \tag{17}$$

and

$$R_T = \frac{Re_\infty k \rho}{\omega \mu}. \tag{18}$$

In Eqn. 17, $F_{onset,s}$ and $F_{onset,cf}$ are onset functions which predict transition onset due to streamwise-aligned instabilities and crossflow respectively. These functions are calculated according to

$$F_{onset,s} = \frac{Re_v}{f(M_e, T_e) Re_{\theta_c}}, \tag{19}$$

and

$$F_{onset,cf} = \frac{\Delta H_{cf} Re_v}{f(M_e, T_e) C_{cf,crit}}, \tag{20}$$

where

$$Re_v = \frac{Re_\infty \rho d^2 S}{\mu}. \tag{21}$$

In these equations, $f(M_e, T_e)$ is a correlation function that converges to the value of 2.2 used by Menter et al. [3] at the incompressible limit. This value is a constant in the Menter γ model. ΔH_{cf} is a modification term based on the local helicity strength (representative of the crossflow strength), and Re_{θ_c} is the critical momentum thickness Reynolds number for transition. These terms are calculated from correlations that are local and algebraic and are formulated by Liu et al. [7] using compressible flat plate data. Included in these correlations are empirical correlations to correct for nose bluntness, local wall temperature ratio, and, in the updated version presented in Ref. [8], pressure gradient. These correlations also rely on local estimates of the boundary-layer edge properties, which are calculated based on the local pressure using a Bernoulli relation, and so assume an isentropic change in properties. The boundary condition for the γ equation is a zero wall-normal gradient. Of the two transition models considered in this work, this model is less complex to implement and has fewer mathematical operations and transport equations. The computational expedience provided by this model is attractive, but the dependence on empirical correlations necessitates the evaluation of the model for test cases outside those presented in Ref. [7], which may have been used to calibrate it in the first place. In this work, the version of the model presented in [7] is used except for in the HIFiRE-1 flight test case where the wall is neither adiabatic nor isothermal at 300 K, the temperature for which the isothermal branch of the baseline version of the model

is tuned. These cases use the extension presented in Ref. [8]. The individual correlations used to calculate the terms of Eqns. 19 and 20 are included in Refs. [7] and [8] and an exhaustive description of the present implementation of the model will be including in forthcoming works which will provide other users all necessary information to implement and verify both models [15] against this OVERFLOW implementation.

D. SST-γ-ν_L Transition Model of Qiao et al. [11]

The second model examined in this work is the high-speed turbulence SST-γ-ν_L model of Qiao et al. [11]. This model includes two additional transport equations coupled to the SST turbulence model, one for the intermittency factor, γ, and one for the eddy viscosity of laminar fluctuations, ν_L. The variable ν_L represents the fluctuations about the laminar base flow that have not yet caused the flow to transition. In calculating the transport of laminar fluctuations leading to instability, this model represents further development of the concepts introduced by Warren and Hassan and extended by Papp and Dash [19–21]. In this model, the value of ν_L is limited to a maximum local nondimensional value of 10 between time steps. The transport equations used in this model are

$$\frac{\partial(\rho\gamma)}{\partial t} + \frac{\partial(\rho u_j \gamma)}{\rho x_j} = P_\gamma - E_\gamma + \frac{1}{Re_r}\frac{\partial}{\partial x_j}\left[(\mu + \mu_t)\frac{\partial\gamma}{\partial x_j}\right] \tag{22}$$

and

$$\frac{\partial(\rho\nu_L)}{\partial t} + \frac{\partial(\rho u_j \nu_L)}{\rho x_j} = P_{\nu_L} - E_{\nu_L} + \frac{1}{Re_r}\frac{\partial}{\partial x_j}\left[\rho\sigma_1(\nu + \sigma_{\nu_L}\nu_L)\frac{\partial\nu_L}{\partial x_j}\right]. \tag{23}$$

The production and destruction terms of the intermittency factor γ are

$$P_\gamma = \rho C_1 F_{onset} S(1-\gamma)[-ln(1-\gamma)]^{\frac{1}{3}} \tag{24}$$

and

$$E_\gamma = \rho C_2 F_{turb}\gamma(C_3\gamma - 1)\Omega. \tag{25}$$

As with the model of Liu et al., the production and destruction of γ is governed by F_{onset} and F_{turb}. The construction of F_{onset} couples the local value of ν_L to the production of γ. All constants used in this model are listed in Table 2. As with other γ models, the turbulence modeling equation is coupled to the transition model through γ only. These functions are defined as

$$F_{onset} = max(F_{onset2} - F_{onset3}, 0) \tag{26}$$

and

$$F_{turb} = exp\left[-(R_T)^4\right], \tag{27}$$

where

$$F_{onset2} = min(max(F_{onset1}, F_{onset1}^4), 2.0), \tag{28}$$

$$F_{onset3} = max(1 - (R_T/3.0)^3, 0) \tag{29}$$

and

$$F_{onset1} = \frac{\nu_L}{C_\mu \nu}. \tag{30}$$

In these equations, R_T is defined according to 18 as with the SST-γ model of Liu et al. [7]. The source terms of the ν_L transport equation are

$$P_{\nu_L} = C_\mu \rho \tau_L S^2 \tag{31}$$

and

$$E_{\nu_L} = \rho\nu\frac{\nu_L}{d^2} \tag{32}$$

where d is the nondimensional distance to the nearest wall, which is limited to nonzero values to avoid a singularity at the wall. For this implementation, the value is limited to 1×10^{-12}. Most of the modeled physics are described by the τ_L parameter, which is the sum of the time scales of the instability mechanisms, as in,

$$\tau_L = \tau_1 + \tau_2 + \tau_{cf} \tag{33}$$

Table 2 Modeling constants for γ transport equations.

C_1	C_2	C_3	C_{2B}	C_{31}	$C_{CF,cr}$	C_μ	σ_1	σ_{ν_L}
100.0	0.06	50.0	0.04802	0074	24.0 (quiet) or 46.0 (noisy)	0.9	1/3	15

Each constituent of the time scale parameter τ_L models the growth of an individual type of instability. This model assumes that a single mode dominates the transition process, and for cases where this is not the case the individual modes contribute additively to transition onset. This is different than the SST-γ model, which tracks modes individually as described by Eqn. 17 and requires that a single onset function exceed the threshold before transition occurs. This model also relies on estimated boundary-layer edge conditions calculated with an isentropic assumption, but does not rely on direct, empirical correlations for nose bluntness, wall temperature ratio, and other factors. Instead, the transport of ν_L is intended to implicitly capture these features. The boundary condition for the γ and ν_L equations is a zero wall-normal gradient. This model requires significantly more calculations per iteration than the SST-γ model discussed in the previous section and includes one more transport equation. This, combined with the fact that this model was found to be more numerically stiff than the previously discussed model, increase its computational cost relative to the other model examined.

In addition to the description of the model provided by Qiao et al. in Ref [11], the authors note the following details of the present implementation:

- The value of σ_{ν_L} is 15, such that the effective coefficient of the diffusion of ν_L is 5.
- The obliqueness angle of the 1^{st} mode instability is calculated in [11] such that the angle is degrees. The angle must be converted to radians for the subsequent correlations to be valid.
- The value of ν_L is restricted to a maximum local nondimensional value of 10.0 at all points in the flow.
- All instances of Re_v in Ref. [11] refer to the local value of strain-based Reynolds number.
- If the local edge Mach number is calculated to be less than 3.8, the 2^{nd} mode time scale, τ_2, is forced to 0.

The individual correlations used to calculate the terms of Eqns. 33 are included in Ref. [11] and an exhaustive description of the present implementation of the model will be including in forthcoming works which will provide other users all necessary information to implement and verify both models against this OVERFLOW implementation [15].

E. OVERFLOW 2.3 Flow Solver

OVERFLOW 2.3 is a structured overset CFD solver capable of conducting time-accurate and steady-state computations. A variety of spatial and temporal discretization options are available in the code. OVERFLOW includes the SST 2003 with the option for transition to be calculated via the Langtry-Menter [2] transition model (SST2003-LM2015). Overflow couples the transition and turbulence modeling equations loosely. At each iteration, the transition modeling equations are solved and the resulting values of γ are used to solve the turbulence modeling equations. For the cases presented here, five turbulence modeling subiterations were taken per flow time step. This study utilizes the release version of OVERFLOW 2.3e as a base and additional transition modeling options coupled to SST are added to the existing capabilities.

III. Test Cases

For this paper, the implementation of the model is evaluated against a selected set of axisymmetric test cases conducted by Liu et al. [7] and Qiao et al. [11] as well as representative test cases not examined by those works. These cases cover both first-mode and second-mode transition and were chosen due to the availability of experimental data in the literature. This section outlines the relevant simulation and the flow parameters of these test cases, and the test case parameters are summarized in Table 3. For each case for which Refs. [7] and [11] provide data, transition modeling inputs were chosen such that computations corresponding the intermediate Reynolds number condition from each experiment could be matched well by the present computations. These inputs were then applied to all other test cases included in an experiment. This allowed for a comparison of the requirements for accurate predictions between the implementation presented in the literature and the one presented here. At the end of this section, results from two test cases not included in the original presentation of the models is provided. For these cases the inputs were selected on a case-by-case basis and the justification for each choice are discussed in the corresponding subsection. These test cases represent a small subset of the work that will be presented in a forthcoming publication [22], which will evaluate the performance of these models for flight test cases as well as for other cases not included in Refs. [7, 8, 11].

A. Numerical Parameters

All simulations performed here were run with a modified version of OVERFLOW 2.3e with the present models implemented. Cases are run with the HLLE++ upwinded scheme [23] with symmetric successive over-relaxation (SSOR) [24] and the van Albada limiter [25]. These computations do not use a quadratic constitutive relation (QCR) or the SST rotational correction to be consistent with Refs. [7, 8, 11]. A grid refinement study is conducted on both models as a first step in analysis, and the results of this are used to inform the grid sizes and y^+ chosen for the cases here. These meshes are found to be more refined than those used by Refs. [7, 8, 11], but it was determined that exactly replicating the meshes used in those references is less important than examining the behavior of the model for cases with adequate resolution for the present implementation. To maintain consistency with the computations of Refs. [7, 8, 11], no sustaining terms are used in these computations. Because the meshes used in these cases are shock-aligned with the inlet located near the nose of the body, this is not expected to significantly impact the solutions. The freestream turbulence and transition modeling inputs are different for each model, and values similar to those presented in Ref. [7] and [11] have been used with each model. An example of the boundary conditions used in these test cases corresponding to a hypersonic cone with isothermal walls is provided in Fig. 1.

B. LaRC Supersonic Cone

The first set of test cases examined in this work is the experiment carried out by Chen et al. [26] on a supersonic cone at various Reynolds numbers. This experiment examined a 5° straight cone with a nose radius of 4 μm and a length of 0.3 m. This test case is used in Refs. [7] and [11] for the initial evaluation of both of the transition models examined here. The experiments studied by this test case were conducted in the NASA Mach 3.5 quiet wind tunnel and are aimed at studying transition driven by Mack's 1^{st} mode. The free-stream conditions across this test campaign are identical for each case except for Reynolds number, which is varied. The wall boundary for this case is nominally adiabatic, and transition is detected in the experiment through the recovery factor, which measures the ratio of the wall temperature to the freestream total temperature and is nominally equal to 0.84 for laminar, calorically perfect air flows, and increases to values near 0.9 upon transition to turbulence. For the SST-γ model, the turbulence modeling conditions for this case are $Tu_\infty(\%) = 0.03$ and $\mu_{T_\infty} = 10.0$, and for the SST-γ-ν_L model they are $Tu_\infty(\%) = 0.1$, $\mu_{T_\infty} = 1.0$, and $\nu_{L_\infty} = 0.05$.

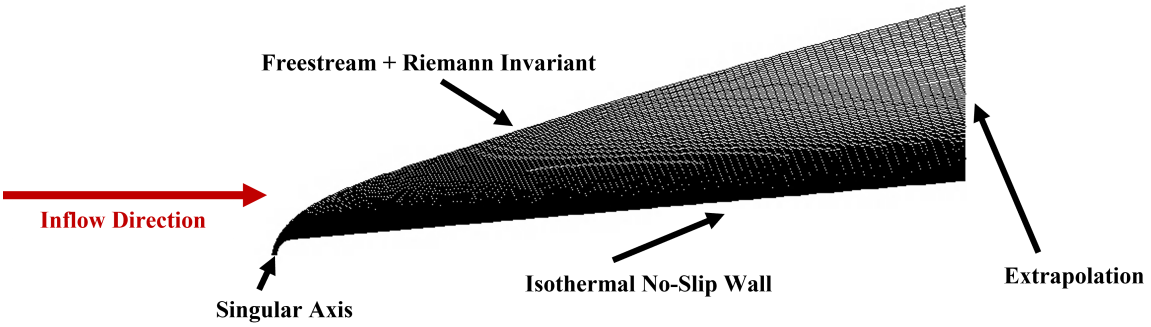

Fig. 1 Representative grid topology and boundary conditions for a test case examined in this work. This mesh corresponds to case LM6b in Table 3.

C. LaRC Hypersonic Cone

The second set of test cases analyzed here corresponds to experiments conducted by Horvath et al. [27] in the NASA Langley Research Center (LaRC) 20-inch Mach 6 test facility. The particular geometry in question is a 5° half-angle cone with a nose radius of 0.00254 mm (0.0001 in). The cone is studied at three different Reynolds numbers corresponding to experimental conditions. The mesh for these cases is a shock-aligned mesh with a maximum initial wall spacing set so that the y^+ for the whole domain remains below 0.25. For the SST-γ model, the turbulence modeling conditions for this case are $Tu_\infty(\%) = 0.4$ and $\mu_{T_\infty} = 10.0$, and for the SST-γ-ν_L model they are $Tu_\infty(\%) = 0.1$, $\mu_{T_\infty} = 1.0$, and $\nu_{L_\infty} = 0.05$.

Table 3 Flow parameters for test cases.

$CaseID$	Configuration	M_∞	$Re_\infty(1/m)$	$T_\infty(K)$	$T_w(K)$	$Tu_\infty(\%)$*	$\mu_{T,\infty}$*	$\nu_{L,\infty}$
LM3p5a	LaRC Mach 3.5	3.5	78.00e6	92.22	adiab.	0.1 (0.03)	1.0 (10.0)	0.05
LM3p5b	LaRC Mach 3.5	3.5	58.90e6	92.22	adiab.	0.1 (0.03)	1.0 (10.0)	0.05
LM3p5c	LaRC Mach 3.5	3.5	49.00e6	92.22	adiab.	0.1 (0.03)	1.0 (10.0)	0.05
LM6a	LaRC Mach 6	6.0	20.30e6	60.56	298.76	0.11 (0.38)	1.0 (10.0)	0.05
LM6b	LaRC Mach 6	6.0	14.10e6	60.56	298.76	0.11 (0.38)	1.0 (10.0)	0.05
LM6c	LaRC Mach 6	6.0	10.50e6	60.56	298.76	0.11 (0.38)	1.0 (10.0)	0.05
LM6d	LaRC Mach 6 Blunt	6.0	25.59e6	60.56	298.76	0.11 (0.38)	1.0 (10.0)	0.05
HF1t20	HIFiRE-1	5.07	18.46e6	201.0	Exp. Dist.	1.0×10^{-4} (0.007)	1.0 (10.0)	2.5×10^{-6}

*Value used for SST - γ-ν_L (Value used for SST-γ)

D. HIFiRE-1 Flight Experiment

The descent phase of the HIFiRE-1 flight test provides transition data for canonical hypersonic geometry at four instances in time, along with the corresponding freestream conditions at those instances [28]. This test been studied computationally at LaRC to identify the stability characteristics corresponding to the transition point [29]. In these prior studies, surface temperature distributions were identified which are used in this study as isothermal wall boundary conditions for the test case. The HIFiRE-1 flight test geometry is a 7 deg half-angle cone with a nose radius of 2.5 mm and a length of approximately 1.1 m. The flight test model includes a cylinder flare section downstream of the cone, but this is not included in the meshes analyzed here. For the HIFiRE flight tests, the turbulence modeling conditions are $Tu_\infty(\%) = 0.007$ and $\mu_{T_\infty} = 10.0$ for the SST-γ model, and they are $Tu_\infty(\%) = 1\times 10^{-4}$, $\mu_{T_\infty} = 1.0$, and $\nu_{L_\infty} = 2.5 \times 10^{-6}$ for the SST-γ-ν_L model. These values were chosen so that the test case corresponding to t = 21 s matched well with experiment. References [7] and [11] do not consider flight test cases, it is left to the present authors to identify appropriate input parameters for these cases.

IV. Results

This section details the results of all the test cases run for this work. First, an exploration of the sensitivities of the models to their input parameters and grid resolution is conducted, along with an investigation of any behaviors of interest resulting from those inquiries. Next, the test cases for which Refs. [7] and [11] provide data for comparison are examined, and then the test cases which for which there is not reference data are presented. Finally, a brief discussion of observations made in the course of conducting this study is provided.

A. Model Evaluation

Before results obtained using the newly implemented model are compared to experimental data or previously published results, a discussion of the characteristics of both models from the user's perspective is warranted. This section details the independent analysis of the model implementations including their grid convergence characteristics, sensitivity to input parameters, and an evaluation of their computational efficiency. For all results in this subsection, the freestream values of the turbulence and transition variables used correspond to those reported by the model authors in Refs. [7, 11]. As such, the transition location and profiles do not necessarily match between the two models. As detailed in Section IV.B, some small changes to the input parameters reported by the model authors were required to achieve agreement with experimental data. In the context of transition modeling, the input parameters are representations of the statistics of the disturbance field at the inflow of the domain, and so it is ideal that the connection between these freestream statistics and the modeling inputs required to model the results of a given test case subjected to that disturbance field be clear and consistent. This section considers only the sensitivities of the model to simulation and grid parameters, and the inputs required to analyze individual test cases are examined in the next section.

1. Grid Independence Study

The first step in evaluating both models was to conduct a grid independence study for both models. A grid independence study confirms that the solution to the discrete model equations for a given problem is independent of the mesh given a necessary level of refinement. Liu et al. [7] present a grid independence study for the LaRC Mach 3.5 cone case, but given that 2^{nd} mode transition prediction is the primary use case of these two models, this study analyzes the grid convergence of the models for one of the LaRC Mach 6 straight cone test cases. The grid levels used in this study are listed in Table 4. The finest grid refinement levels used in this study are significantly more refined than would be seen in a typical RANS calculation for production CFD runs.

The results of the grid independence study are shown in Fig 2. It is observed that for this test case the SST-γ-ν_L model of Qiao et al. [11] requires significantly less refinement to grid converge than the SST-γ model of Liu et al. [7]. The level of refinement required for formal grid convergence for the latter approaches that of meshes typically used for LES simulations. Still, provided sufficient grid resolution, both models yield grid converged results. It is observed that the SST-γ-ν_L model predicts lower surface heating values in the turbulent region than the corresponding predictions of fully turbulent simulations. It is possible that this underprediction is the result of the appreciable value of ν_L in the boundary layer downstream of transition altering the value of the onset function described by Eqn. 30 and preventing production of γ in the lower parts of the boundary layer compared to the SST-γ model. Further work is required to fully investigate this phenomenon, and to identify possible corrections.

The $\gamma - \nu_L$ model also exhibits a post-transition bump in the skin heating in one of the grid refinement cases. For this case, the transition modeling variable ν_L is observed to diverge at this point in the flow. Because ν_L is limited to a maximum nondimensional value of 10, the divergence of this quantity does not cause divergence of the solution, and causes the observed spike in turbulent quantities shown in the grid convergence results.

2. Sensitivity to Turbulence Model Version

As both of these models are constructed to be coupled with the SST turbulence model, it is necessary to evaluate the relative importance of the version of the SST turbulence model the transition model is coupled with. The SST turbulence model has two commonly used versions, one released in 1994 [17] and an updated version released in 2003 [3]. It is desirable that the SST model version have negligible impact on the transition predictions of a transition model. Both models examined here are coupled with the 1994 version of SST, but OVERFLOW currently includes the 2003 version of the model. To evaluate the influence of the version of the SST model used, both versions are coupled to each transition model and the results for the LaRC Mach 6 cone are compared. This comparison is presented in Fig. 3. It is observed that the SST-$\gamma - \nu_L$ model of Qiao et al. [11] is insensitive to the version of SST used, but the SST - γ model of Liu et al. [7] is. This sensitivity may be traced to the difference in the limiter applied to the turbulent kinetic energy production equation. The 2003 update to the model reduces the maximum local production of k from 20 to 10, which for the SST-γ model results in delayed transition. For the remainder of the cases examined, the 1994 version of SST is used with both transition models.

B. Comparison to Results from Original Model Developers

This section presents test cases which are also included in the original presentation of both models by the respective model developers. These correspond to the experiments of Chen [26] and Horvath [27], and were presented as a demonstration of each model's ability to capture 1^{st} and 2^{nd} mode dominated transition respectively. However, it is not

Table 4 Grid levels for grid refinement study.

Level	I × J	wall y^+
1	257 × 193	0.3
2	385 × 289	0.2
3	513 × 385	0.15
4	769 × 579	0.1
5	1025 × 769	0.08
6	1573 × 1153	0.05

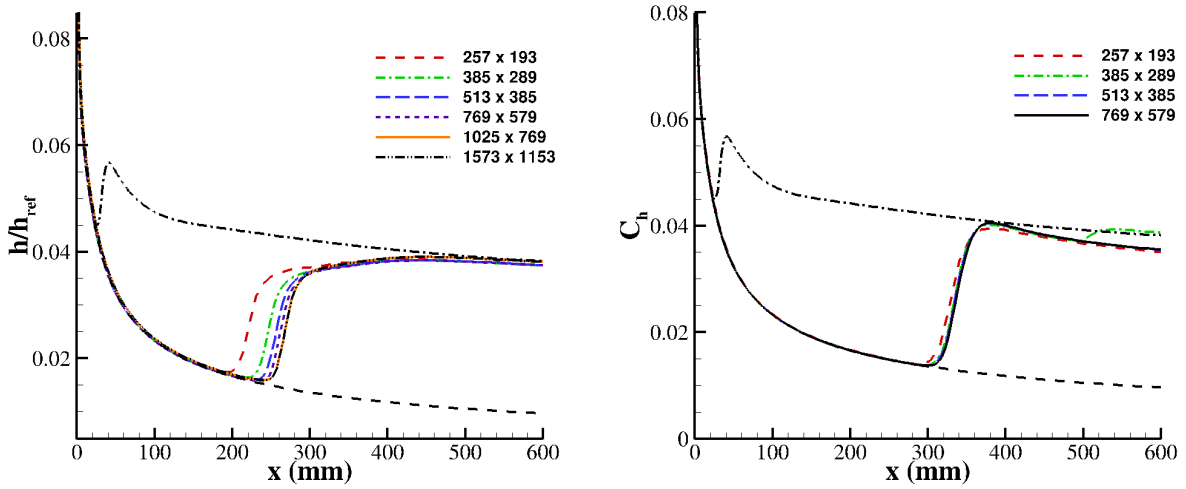

a) SST - γ model

b) SST - $\gamma - \nu_L$ model

Fig. 2 Evaluation of grid convergence for the surface heat transfer calculated in OVERFLOW with both compressible transition models. The case examined is the LM6b case from Table 3 for which Re_∞ = 14.1$\times$ 10^6/m, M_∞ = 6, and the freestream transition modeling inputs are given in Table 3. The dashed and dashed-dotted lines are included as a reference and correspond to the heat transfer predictions for the laminar and fully-turbulent cases, respectively.

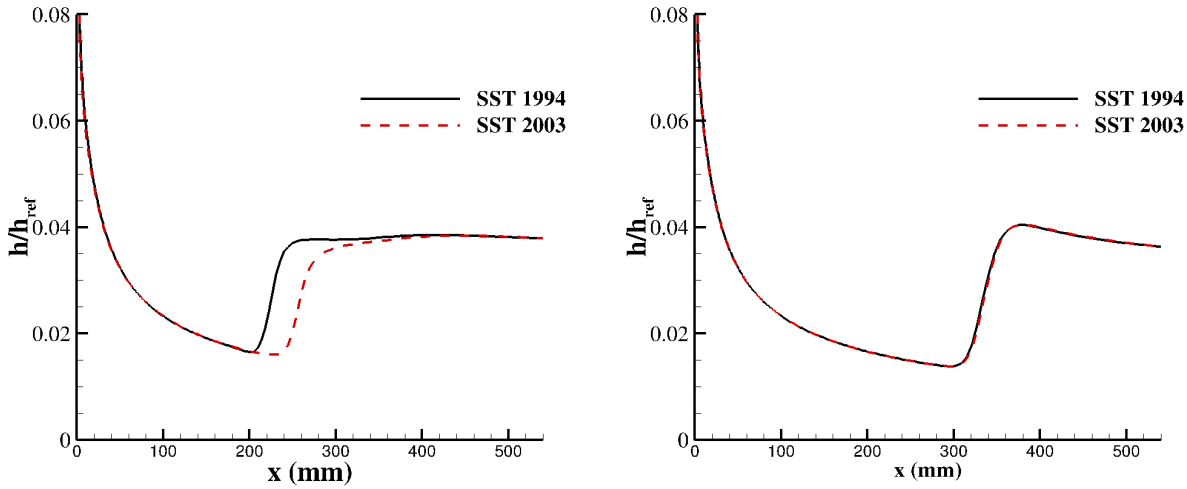

(a) SST - γ model

(b) SST - $\gamma - \nu_L$ model

Fig. 3 Comparison between transitional heat transfer predictions with SST 1994 and SST 2003. The case examined is the LM6b case from Table 3 for which M_∞ = 6, Re_∞ = 14.1$\times$ 10^6/m and the freestream transition modeling inputs are given in Table 3.

clear if these test cases were used in any way in the calibration of either model. These test cases are presented one model at a time, and any differences between the parameters required in this analysis and those presented in Refs. [7, 11] are noted in the text. For these cases, the 1994 version of SST is used and no modifications are made to the original models (such as changing σ_{ν_L}). The grid refinement study of a single test case presented in the prior section is used to guide the mesh choice for subsequent cases. For the SST-γ-ν_L model, meshes similar in resolution to the 513 $\times$ 385 meshes are

used, and for the SST-γ model, meshes based on the the 1025 $\times$ 769 mesh is used. Forthcoming work will present more detailed grid convergence data for cases LM3p5a - LM3p5c and LM6a - LM6c of Table 3 [15]. The transition locations are found to be those of the experiment, but the transition zone regions are predicted to be narrower than those seen in the tunnel data.

1. *SST-γ Model [7]*

The results for the SST-γ model are compared to the LaRCh Mach 3.5 experiment [26] in Fig. 4. Liu et al. [7] provide skin friction data which indicates the transition region just as the recovery factor does, but in this work recovery factor is presented as well as skin friction for consistency with the experiment. Good agreement is found using Tu_∞ = 0.03, which is slightly larger than the value used by Liu et al. [7] of Tu_∞ = 0.02, and μ_T = 10 is used.

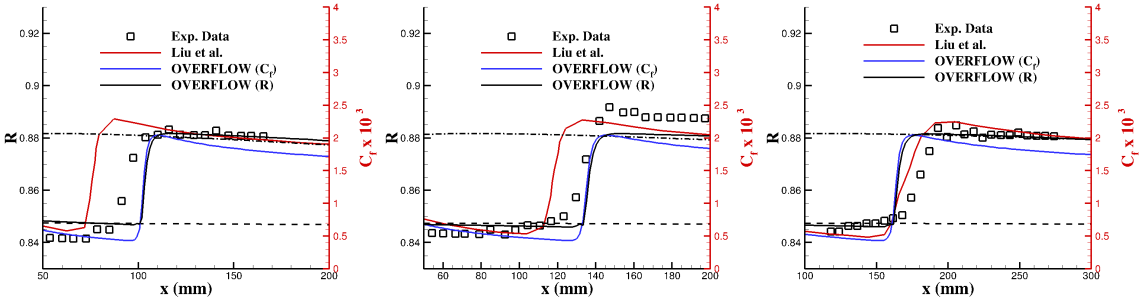

(a) Re = 78.0$\times$ 10^6/m (b) Re = 58.9$\times$ 10^6/m (c) Re = 38.5$\times$ 10^6/m

Fig. 4 Prediction of recovery factor and skin friction using the SST-γ model for the LaRC Mach 3.5 cone cases corresponding to cases LM3a, LM3b, and LM3c in Table 3. For these cases, the wall is treated as adiabadic, M_∞ = 3.5 and the other freestream parameters are described in Table 3.The dashed and dashed-dotted lines are included as a reference and correspond to the heat transfer predictions for the laminar and fully-turbulent cases, respectively. In this plot, the results reported by Liu et al. [7] are for skin friction, but the experimental data provided are in terms of recovery factor.

The results of the SST-γ model for the LaRC Mach 6 cone are shown in Fig. 5. For this case, the input parameters were Tu_∞ = 0.38 and μ_{T_∞} = 10.0. The slope of the transition region in this study was found to be slightly steeper than that reported by Liu et al., and the slope was found to be insensitive to $\mu_{T_\infty} > 2.0$. Once again, agreement found in this case is good overall. One observation made in this hypersonic cone case is the tendency of the SST-γ model to exhibit a biphasic transition region. The initial steep region of transition nearly achieves the turbulent heat flux level but is followed by a second region where the heat flux is increasing slowly before peaking and then descending again.

2. *SST-γ-ν_L Model [11]*

Results for the three LaRC Mach 3.5 cone cases compared both to the experimental data and to the digitized version of the results from Ref. [11] is presented in Fig. 6. This case is run with input parameters identical to Ref. [11]. Namely, μ_L = 0.05, μ_T = 1.0, and Tu_∞ = 0.1. In the turbulent region the results calculated with OVERFLOW show good agreement with the experimental data, and the present implementation is found to be noticibly less sensitive to the freestream Reynolds number than that of Qiao et al. [11]. It was mentioned in the discussion of the grid independence study that this model does not fully reach the turbulent surface heating and/or skin friction in many cases. It should be noted that, while Qiao et al. do not provide fully turbulent results using their CFD solver, the behavior observed in these figures, in particular Fig. 6, suggest that the results presented in Ref. [11] do not exhibit the behavior expected from a fully turbulent SST solution in the region downstream of transition. In the case of the Mach 3.5 cone, the reported recovery factor increases continually downstream of transition, and in the case of the Mach 6 cone, soem cases demonstrate significant overestimation of the fully turbulent heat transfer. Neither of these behaviors is observed in some of the turbulent region of the simulations conducted for this study.

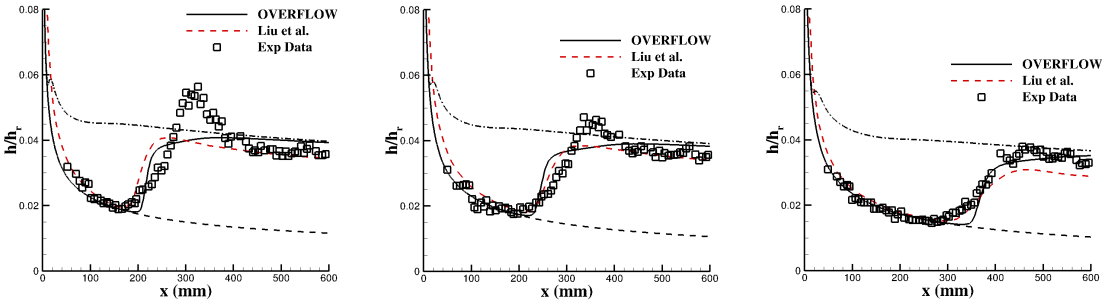

(a) Re = 20.3 × 10^6/m (b) Re = 14.1× 10^6/m (c) Re = 9.2× 10^6/m

Fig. 5 Prediction of heat transfer using the SST-γ model for the LaRC Mach 6 cone cases corresponding to cases LM6a, LM6b, and LM6c in Table 3. For these cases, the wall is treated as isothermal with T_w = 300 K, M_∞ = 6.0 and the other freestream parameters are described in Table 3.The dashed and dashed-dotted lines are included as a reference and correspond to the heat transfer predictions for the laminar and fully-turbulent cases, respectively.

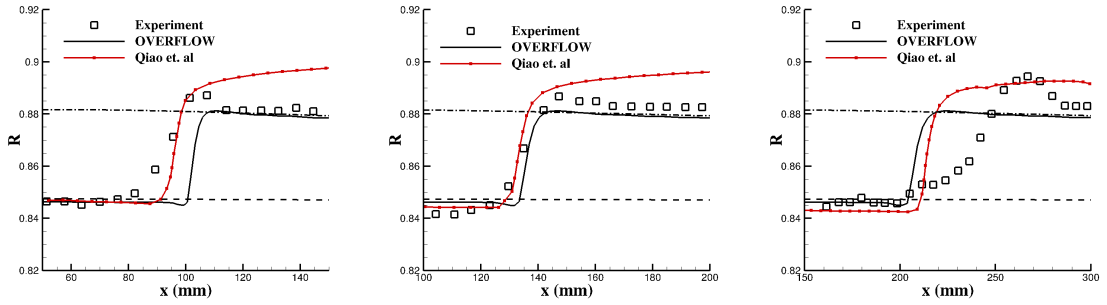

(a) Re = 78.0× 10^6/m (b) Re = 58.9× 10^6/m (c) Re = 38.5× 10^6/m

Fig. 6 Prediction of recovery factor and skin friction using the SST-γ-ν_L model for the LaRC Mach 3.5 cone cases corresponding to cases LM3a, LM3b, and LM3c in Table 3. For these cases, the wall is treated as adiabadic, M_∞ = 3.5 and the other freestream parameters are described in Table 3.The dashed and dashed-dotted lines are included as a reference and correspond to the heat transfer predictions for the laminar and fully-turbulent cases, respectively.

For the LaRC Mach 6 cone, shown in Fig. 7, good agreement with the experiment and coupled results from Ref. [11] was found by taking Tu_∞ = 0.11 rather than the 0.1 used by Qiao et al. This adjustment is small, and the difference is attributed to potential differences in solver, as all other modeling parameters are the same as for Ref. [11] Overall, good agreement with the transition locations predicted in the experiment and reported by Qiao et al. [11] is seen here as well, and the post-transition increase in heat transfer observed in the results of Qiao et al. [11] is not observed here.

Across all these test cases, the present implementations exhibit behaviors that are broadly consistent with the experimental data underpinning them and the computational data of Qiao and Liu [7, 11]. However, it is worth noting that both models predict relatively narrow transition zones in comparison with the experimental data. Neither model is able to capture the pronounced overshoot in heat transfer near the end of the transition region.

C. Additional Test Cases

This section outlines the results for additional test cases that were not examined in the original presentation of either model. This exercise is necessary to provide an unbiased evaluation of the models to ensure that the models are applicable to general test cases. The test cases presented here are chosen to evaluate the performance of the models in a variety of Mach numbers and freestream noise environments. Included in the presentation of these results is a discussion of the input parameters required to achieve them. When working in the transition modeling space, it should

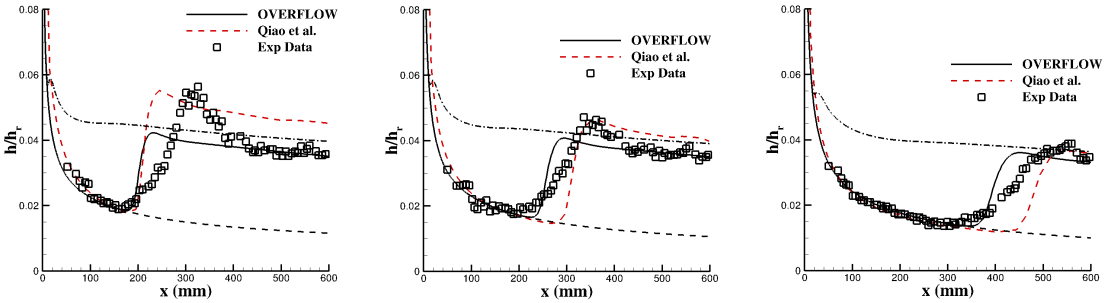

(a) Re = 20.3 × 10^6/m (b) Re = 14.1× 10^6/m (c) Re = 9.2× 10^6/m

Fig. 7 Prediction of heat transfer using the SST-γ-ν_L model for the LaRC Mach 6 cone cases corresponding to cases LM6a, LM6b, and LM6c in Table 3. For these cases, the wall is treated as isothermal with T_w = 300 K, M_∞ = 6.0 and the other freestream parameters are described in Table 3.The dashed and dashed-dotted lines are included as a reference and correspond to the heat transfer predictions for the laminar and fully-turbulent cases, respectively.

be noted that nearly any given result case can be achieved by tuning the input parameters. However, in order for a model to be useful in making predictions, a user must be able to estimate the input parameters based on the flow conditions without tuning for each seperate test case. Therefore, the models are first evaluated based on whether or not they can reproduce the experimental solution to these test cases, and then based on whether or not the required inputs to do so are similar to those used for other test cases involving similar facilities or flight conditions. A detailed description of the results obtained for these additional test cases is provided in Ref. [15], here, we simply summarize a few key findings of that work.

The LaRC cone with a slightly blunted nosetip was part of the same experimental campaign as the other LaRC Mach 6 cone cases presented in Refs. [7, 11]. Liu et al include this case in their write-up of the model because their SST-γ model includes specific corrections for nose bluntness, but the SST-γ-ν_L model does not include such a correction and does not present this test case [11]. The inflow parameters for this case were chosen to be identical to those used for the other LaRC Mach 6 cone cases and the results plotted in Fig. 8 demonstrate that both models are able to mimic the trends from the experimental experiments. This is particularly noteworthy for the SST-γ-ν_L model, as it indicates that the transport of ν_L is able to capture the impact of nose bluntness on transition without an empirical correction built into the model.

Examination of flight test data is of particular importance in evaluating high-speed transition models as the design of flight vehicles is the primary end-user application for the models. Because much of the transition data obtained in ground facilities is based on high noise environments, those data cannot be easily extrapolated to flight and the transition model must be able to make predictions for both environments. Additionally, the models analyzed here do not include flight test cases in their original presentation, and so it is necessary to evaluate what input parameters are necessary to replicate flight transition. The flow conditions and surface temperature distributions for these HIFiRE flight test cases are the same as those used by Li et al. [29]. The results for the comparison of the CFD predictions with the flight test data are shown in Fig. 9. To achieve agreement with the experiment, the SST-γ-ν_L model required μ_{L_∞} = 2.5 $\times 10^{-6}$ and Tu_∞ = 1.0 × 10^{-4}. Because this test case required an alteration to the freestream value of μ_L, this quantity can't be considered a universal parameter as implied by the test cases in Ref. [11]. For the SST-γ model, Tu_∞ = 0.007 was required. For both of these models, the inputs required to replicate flight conditions correspond to lower levels of freestream noise than is the case for the noisy and quiet tunnel cases.

V. Summary and Concluding Remarks

First, a summary of the findings is provided, followed by conclusions based on those observations. Finally, recommendations for future work in the development of high-speed transport models is provided.

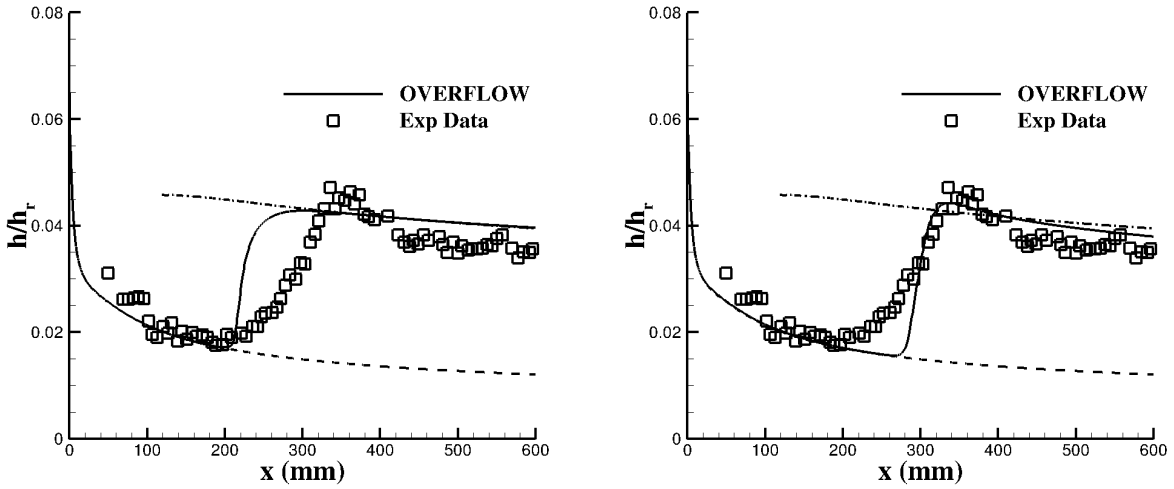

(a) SST-γ model

(b) SST-γ-ν_L model

Fig. 8 Prediction of heat transfer for the LaRC Mach 6 cone case with R_N = 1.6 mm corresponding to case LM6d in Table 3. For these cases, the wall is treated as isothermal with T_w = 300 K, Re = 25.6 $\times$ 10^6/m, M_∞ = 6.0 and the other freestream parameters are described in Table 3. The dashed and dashed-dotted lines are included as a reference and correspond to the heat transfer predictions for the laminar and fully-turbulent cases, respectively.

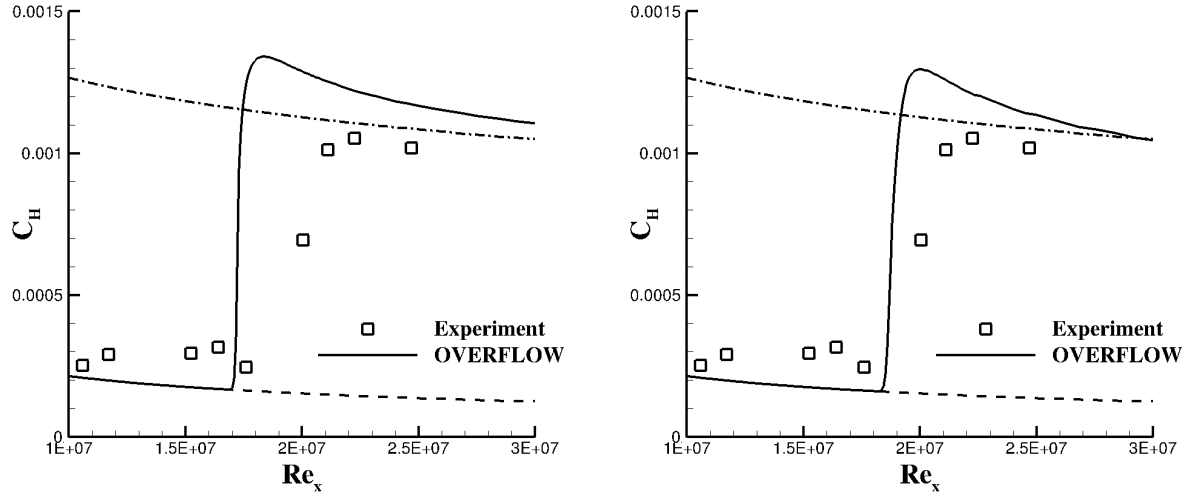

(a) SST-γ model

(b) SST-γ-ν_L model

Fig. 9 Predicted heat transfer profiles for the HIFiRE-1 flight test case (t = 20 s) with the SST - $\gamma - \nu_L$ model. For the flight case, surface temperature distribution is based on the paper by Li et al. [29] and all freestream parameters are provided in Table 3. The dashed and dashed-dotted lines are included as a reference and correspond to the heat transfer predictions for the laminar and fully-turbulent cases, respectively.

A. Summary

Prediction of laminar-turbulent transition is an important capability for hypersonic CFD applications, and at present there is a gap between the tools developed by the research community and those available to designers in industrial CFD codes. This manifests as a large volume of published but not yet broadly implemented models, which must be vetted by

the community before they see mass adoption. The results presented here represent a preliminary assessment of two high-speed transport models, namely an SST-γ transition model [7] and an SST-γ-ν_L model [11]. A description of each model is provided, including the limiters and other supplementary information required to implement them. Both models are used to predict surface heating and/or skin-friction distributions for a suite of test cases using high-quality, shock-aligned meshes with characteristic values of y^+ at or below 0.1. These cases included some cases that were included with the original presentations of these models (and could have potentially been used for model calibration) as well as additional test cases that may provide a blind assessment of the models. In particular, both transition models have been applied to flight configurations for the first time and the results indicate that, with suitable calibration, these models could be applied for engineering predictions of in-flight transition.

B. Conclusions

Both of these models demonstrate a reasonable ability to predict laminar-to-turbulent transition in canonical hypersonic and supersonic flow scenarios. By way of comparison, the SST-γ model [7] is easier to implement and computationally robust, but slow to grid converge and is reliant on empirical correlations to capture the effects of nose radius and wall temperature. The SST-γ model also demonstrates senstivity to the version of SST used, and so would need slight recalibration for use with SST 2003. The SST-γ-ν_L model requires more computational resources than similar models and is numerically less robust, but grid converges with lower resolution than the other model and gives reliable predictions without needing purely empirical correlations. While both models work well for the canonical cases studied herein, the findings here suggest that the SST-γ-ν_L framework may be better positioned toward further advancement for general applications. The SST-γ-ν_L model provided reasonable predictions across all test cases and, as desired, was insensitve to inputs settings such as the choice of the version of the SST model used. This model was found to reasonably predict the delay in transition caused by nose bluntness without the need for an explicit correlation requiring the input of the nose bluntness parameter. Its principle shortcoming is numerical stiffness of the ν_L transport equation and the transition modeling community has experience applying corrections to models to address similar numerical limitations. Neither model predicts overshoot of turbulent heat transfer in cases where that phenomenon is observed experimentally, and both models predict narrower transition regions than are observed in experiments for most cases.

C. Recommendations for Future Work

Using isentropic relationships to relate the freestream parameters to the boundary layer edge quantities is an inherently limited approach. This assumption can lead to inaccurate reference information for the the local correlations in the transition models. However, some method of estimating the edge quantities based on the local quantities within the boundary layer is required. Currently, aside from that of the references examined here, the only readily available method for this estimation is to use oblique or conical shock theory to analytically calculate the inviscid flow conditions, assuming a single oblique or conical shock to achieve the local pressure from the freestream. Other methods, even heuristic ones, are of interest for the continued development of this class of transition model.

For the SST-γ-ν_L model, it is observed in some cases that the ν_L transport equation is prone to divergence early in the simulation, which can prevent the simulation from arriving at accurate predictions. It was found that the value of the diffusion coefficient, σ_{ν_L}, could be lowered to stabilize the model and allow certain test cases to be analyzed which could not have been run with the baseline version. However, the impact of this change, both in terms of the potential computational speedup and the impact on the predicted transition characteristics should be investigated. The resolution of this problem is necessary for this or similar models to be useful for general applications, and future works will investigate this behavior in greater detail.

As models are matured towards general applicability, care must be taken to ensure that each model exhibits a clear and consistent relationship between freestream disturbance statistics and the input parameters to the transition model. Some inconsistencies in this interpretation are observed for the The SST-γ-ν_L model in particular, and this ambiguity is expected to become more prevelant as additional test cases considering the complete range of instability type and facility or environment noise level are examined. It is suggested that this model be examined in light of the existing correlations for estimating the turbulent kinetic energy from a tunnel's free stream noise [30, 31] to ensure that the model can be applied without a priori knowledge of Tu_∞ and ν_{L_∞}.

Finally, while both models are able to accurately predict transition location for most cases, the shape of the transition zone, particularly its extent and the overshoot observed in some experiments, is not captured in general for these cases. In further developing the transition models for high-speed flows, it is of interest to add this capability to those models.

Acknowledgments

This research is sponsored by the NASA Hypersonic Technology Project (HTP) and the NASA Transformative Tools and Technologies Project (TTT) under the Aeronautics Research Mission Directorate. The research of Balaji Venkatachari is funded by the NASA Langley Research Center through the cooperative agreement 2A00 with the National Institute of Aerospace (NIA). Computations included in this work were utilized the LaRC K midrange supercomputing cluster along with the computational resources provided by the NASA High-End Computing (HEC) Program through the NASA Advanced Supercomputing (NAS) Division at the Ames Research Center.

References

[1] Menter, F. R., Langtry, R., and Völker, S., "Transition Modelling for General Purpose CFD Codes," *Flow Turbulence and Combustion*, Vol. 77, 2006, pp. 277 – 303. https://doi.org/10.1007/s10494-9047-1.

[2] Menter, F., Smirnov, P. E., Liu, T., and Avancha, R., "A One-Equation Local Correlation-Based Transition Model," *Flow, Turbulence and Combustion*, Vol. 95, 2015, pp. 583–619.

[3] Menter, F., Kuntz, M., and Langtry, R. B., "Ten Years of Industrial Experience with the SST Turbulence Model," *Journal of Heat and Mass Transfer*, Vol. 4, 2003.

[4] Coder, J. G., Pulliam, T. H., and Jensen, J. C., "Contributions to HiLiftPW-3 Using Structured, Overset Grid Methods," *AIAA Scitech Forum 2018*, 2018. https://doi.org/10.2514/6.2018-1039.

[5] Spalart, P. R., and Allmaras, S. R., "A One-Equation Turbulence Model for Aerodynamic Flows," *Recherche Aerospatiale*, Vol. 1, 1994, pp. 5 –21.

[6] Anderson Jr, J. D., *Hypersonic and High-Temperature Gas Dynamics*, American Institute of Aeronautics and Astronautics, 2019. https://doi.org/10.2514/4.105142, 3rd Edition.

[7] Liu, Z., Lu, Y., Li, J., and Yan, C., "Local Correlation-Based Transition Model for High-Speed Flows," *AIAA Journal*, Vol. 60, 2022. https://doi.org/10.2514/1.J060994.

[8] Liu, Z., Lu, Y., Xiao, F., and Yan, C., "Local Correlation-Based Transition Model for High-Speed Flows," *AIAA Journal*, 2022. https://doi.org/10.2514/1.J061585, article in Advance.

[9] Qiao, L., Bai, J.-Q., adn Jing-Lei Xu, J.-K. X., and Zhang, Y., "Toward a Practical Method for Hypersonic Transition Prediction Based on Stability Correlations," *International Journal of Nonlinear Sciences adn Numerical Simulation*, Vol. 47, No. 10, 2018. https://doi.org/10.1515/ijnsns-2017-0011.

[10] Qiao, L., Xu, J., Xu, J., and Zhang, Y., "Modeling of Supersonic/Hypersonic Boundary Layer Transition Using a Single-Point Approach," *International Journal of Nonlinear Sciences and Numerical Simulation*, Vol. 11, 2019. https://doi.org/10.1515/ijnsns-2017-0011.

[11] Qiao, L., Xu, J., Bai, J., and Zhang, Y., "Fully Local Transition Closure Model for Hypersonic Boundary Layers Considering Crossflow Effects," *AIAA Journal*, Vol. 59, No. 5, 2021. https://doi.org/10.2514/1.J059765.

[12] Diviaharshavardini, R. C., Prakash, K. A., and Rajesh, G., "An All-Speed Formulation using a modified γ-Model for the Prediction of Boundary Layer Transition and Heat Transfer," *International Journal of Heat and Mass Transfer*, Vol. 195, 2022. https://doi.org/10.1016/j.ijheatmasstransfer.2022.123121.

[13] Xu, J., Bai, J., Fu, Z., Qiao, L., Zhang, Y., and Xu, J., "Parallel Compatible Transition Closure Model for High-Speed Transitional Flow," *AIAA Journal*, Vol. 55, 2017. https://doi.org/10.2514/1.J055711.

[14] Nichols, R. H., and Buning, P. G., *User's Manual for OVERFLOW 2.3*, NASA Langley Research Center, Hampton, VA, October 2019. URL https://overflow.larc.nasa.gov/.

[15] Vogel, E. A., Venkatachari, B. S., and Choudhari, M., "Verification of Two High-Speed Transition Models in OVERFLOW," 2023. In Preparation.

[16] Rumsey, C. L., "Compressibility Considerations for κ-ω Turbulence Models in Hypersonic Boundary Layer Applications," , 2009. NASA/TM–2009-215705.

[17] Menter, F., "Two-equation Eddy Viscosity Turbulence Models for Engineering Applications," *AIAA Journal*, Vol. 32, No. 8, 1994.

[18] Venkatachari, B. S., Gosin, S., and Choudhari, M., "Implementation and Assessment of Menter's Galilean-Invariant γ Transition Model in OVERFLOW," *AIAA Aviation Forum 2023*, American Institute of Aeronautics and Astronautics, 2023. Preprint.

[19] Warren, E. S., Harris, J. E., and Hassan, H. A., "Transition Model for High-Speed Flow," *AIAA Journal*, Vol. 33, No. 8, 1995. https://doi.org/10.2514/3.12687.

[20] Warren, E. S., and Hassan, H. A., "Transition Closure Model for Predicting Transition Onset," *Journal of Aircraft*, Vol. 35, No. 5, 1998, pp. 769 – 775.

[21] Papp, J. L., and Dash, S. M., "Hypersonic Transitional Modeling for Scramjet and Missile Applications," *40th AIAA Aerospace Sciences Meeting and Exhibit*, 2002. https://doi.org/10.2514/6.2002-155.

[22] Vogel, E. A., Venkatachari, B. S., and Choudhari, M., "Validation of SST -γ and SST - $\gamma - \nu_L$ Transition Models for High-Speed Flows," 2023. In Preparation.

[23] Park, S. H., Lee, J., and Kwon, J., "Preconditioned HLLE Method for Flows of all Mach numbers," *AIAA Journal*, Vol. 44, No. 11, 2006, pp. 2645 – 2653.

[24] Krishna, L. B., "On the Convergence of the Symmetric Successive Overrelaxation Method," *Linear Algebra and its Applications*, Vol. 56, No. 1, 1984, pp. 185 – 194.

[25] van Albada, G. D., van Leer, B., and Jr., W. W. R., "A Comparative Study of Computational Methods in Cosmic Gas Dynamics," *Astronomy and Astrophysics*, Vol. 108, No. 1, 1982, pp. 76 – 82.

[26] Chen, F.-J., Malik, M. R., and Beckwith, I. E., "Boundary-Layer Transition on a Cone and Flat Plate at Mach 3.5," *AIAA Journal*, Vol. 27, No. 6, 1989.

[27] Horvath, T. J., Berry, S. A., Hollis, B. R., Chang, C.-L., and Singer, B. A., "Boundary Layer Transition on Slender Cones in Conventional and Low Disturbance Mach 6 Wind Tunnels," *32nd Fluid Dynamics Conference and Exhibit*, American Institute of Aeronautics and Astronautics, 2002.

[28] Kimmel, R. L., Adamczak, D., Paull, A., Paull, R., Shannon, J., adn Myles Frost, R. P., and Alesi, H., "HIFiRE-1 Ascent-Phase Boundary-Layer Transition," *Journal of Spacecraft and Rockets*, Vol. 52, No. 1, 2015. https://doi.org/10.2514/1.A32851.

[29] Li, F., Choudhari, M., Chang, C.-L., Kimmel, R., Adamczak, D., and Smith, M., "Transition Analysis for the Ascent Phase of HIFiRE-1 Flight Experiment," *Journal of Spacecraft and Rockets*, Vol. 52, No. 2, 2015, pp. 1283 – 1293. https://doi.org/10.2514/1.A33258.

[30] Wang, L., and Fu, S., "Development of an Intermittency Equation for the Modeling of the Supersonic/Hypersonic Boundary Layer Flow Transition," *Flow, Turbulence, and Combustion*, Vol. 87, 2011, pp. 165–187. https://doi.org/10.1007/s10494-011-9336-1.

[31] He, Y., and Morgan, R. G., "Transition of Compressible High Enthalpy Boundary Layer Flow Over a Flat Plate," *The Aeronautical Journal*, Vol. 98, No. 972, 2016, pp. 25–34. https://doi.org/10.1017/S0001924000050181.